Materials Chemistry and Physics 240 (2020) 122137

Contents lists available at ScienceDirect

Materials Chemistry and Physics

journal homepage: www.elsevier.com/locate/matchemphys

A convenient co-precipitation method to prepare high performance $LiNi_{0.5}Mn_{1.5}O_4$ cathode for lithium ion batteries

Yidong Shen, Xiaokang Ju, Jinzhu Zhang, Tingzhen Xie, Fengyi Zong, Dongyang Xue, Xiaopin Lin, Jianmin Zhang, Qiuhong Li *

Pen-Tung Sah Institute of Micro-Nano Science and Technology, Xiamen University, Xiamen, 361005, China

HIGHLIGHTS

- Multilevel spherical material $LiNi_{0.5}Mn_{1.5}O_4$ was prepared by coprecipitation and following gradient temperature calcination.
- The precursors could be obtained within an hour with proper portion of ethanol and water as cosolvent.
- The cathode exhibited stable retention above 94% over 200 cycles at 1C and high rate capacities.

GRAPHICAL ABSTRACT

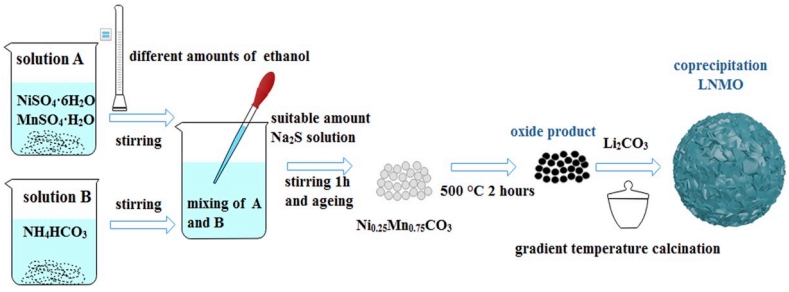

ARTICLE INFO

Keywords:
$LiNi_{0.5}Mn_{1.5}O_4$
Multilevel spherical material
Dielectric constant
Cathode material

ABSTRACT

A convenient and fast strategy to construct multistage spherical $LiNi_{0.5}Mn_{1.5}O_4$ by coprecipitation and following gradient temperature calcination has been developed. Considering about the effect of reaction kinetics, ethanol and water were used as co-solvent to accelerate the crystallite nucleation and reduce the reaction time. The precursors could be obtained within an hour with ethanol/water proportion of 1:3. Due to the synergistic effect of nanoscale primary particles and assembled micro-spheres of hierarchical $LiNi_{0.5}Mn_{1.5}O_4$ product, the material showed high electrochemical properties as cathode for lithium ion batteries. The cathode delivered 141 mAh g^{-1} at 1 C and maintained 94.2% after 200 cycles. Even at 10 C, 114 mAh g^{-1} could be retained. Furthermore, the full cell with $Li_4Ti_5O_{12}$ delivered 132.4 mAh g^{-1} at 1 C and kept 92.4% retention after 200 cycles. And the product at 55 °C also exhibited 133.2 mAh g^{-1} at 1 C and kept 93.2% after 100 cycles.

1. Introduction

For the past few years, rechargeable lithium batteries have been applied to many aspects including electric vehicles, hybrid electric vehicles and portable electronic products because of their high energy density, long cruising autonomy and good environmental friendliness. Nowadays, they have obtained a great deal of attention and support from the state and the society. However, with the increasing requirements of the industrial production, outstanding cathode materials which can provide higher capacity or higher voltage are demanded [1–7].

Compared with the conventional cathode materials such as $LiCoO_2$ and $LiFePO_4$, the high voltage cathode material, $LiNi_{0.5}Mn_{1.5}O_4$ (LNMO), possesses a voltage plateau of 4.7 V, which means the amount

* Corresponding author.
E-mail address: liqiuhong@xmu.edu.cn (Q. Li).

https://doi.org/10.1016/j.matchemphys.2019.122137
Received 24 May 2019; Received in revised form 14 August 2019; Accepted 7 September 2019
Available online 7 September 2019
0254-0584/

of cathode materials to set up a battery pack can be reduced. Consequently, the industries can bring down the cost of manufacture by using this kind of material. Furthermore, LNMO exhibits a great preponderance with higher energy density of 650 Wh kg^{-1}, which compares to the 500 Wh kg^{-1} of $LiMn_2O_4$, 540 Wh kg^{-1} of $LiFePO_4$ and 540 Wh kg^{-1} of $LiCoO_2$ [8,9].

The prominent properties of this material have attracted much attention, and many synthetic methods have been reported, which include hydrothermal method, sol-gel method, template method, spray drying, coprecipitation method, solid-state method and so on [10–26]. However, the synthesis processes have companied with long period, low output and rigorous conditions. They are still difficult to be widely used in mass production for commercialization.

In this paper, we will introduce a quite convenient and efficient coprecipitation method to synthesize $LiNi_{0.5}Mn_{1.5}O_4$ with a spherical multistage structure. And the precursor of LNMO can be prepared in an hour. During the process, the dielectric constant of reaction kinetics plays an important role. According to the formula of the reaction kinetics of solution, the relationship between dielectric constant (ε) and reaction rate constant (k) could be concluded to that: $\{\partial \ln K/\partial(1/\varepsilon)\}_T = Z_A Z_B Le^2/RTa$ (The derivation of the formula is shown in Supplementary Material), where Z represents the valence, L represents the Avogadro constant, e means the electron charge, a stands for the ion diameter, T is the temperature, and R is referred to the ideal gas constant. According to this formula, it's not difficult to discover that the decreasing dielectric constant can accelerate the kinetics process of the combination reaction. Furthermore, the dielectric constant influences the nucleation and growth of the crystalloid. The dielectric constants of distilled water and ethanol are 81 and 26 respectively at room temperature. When we adopt distilled water and ethanol as mixed solvent, the dielectric constant of solution would be reduced the and the reaction rate would be increased. The dielectric constant is around 60 at the proportion of ethanol to water is 1:3. In this way, alcohol reduces the dielectric constant significantly and hence, the rate of reaction is also strengthened [27–29]. Under this reaction condition, we will shrink the time cost and increase the output.

On the other hand, since some reactants can not be dissolved very well in ethanol, the varying of dielectric constants will have an effect on the solubility and the supersaturation of solute, which will affect the crystal growth and the interaction between solute and solvent. We need an appropriate amount of distilled water to make up this shortage. Therefore, the proportion of ethanol to distilled water shall be adjusted to achieve an optimal reaction environment. And the final product exhibits an excellent structure. The nanoscale primary particles of the material contribute to the enhancement of the rate performance, while the assembled micron-scale secondary particles benefit to the cyclic stability.

We also prepared LNMO cathode by a conventional sol-gel method for comparison. The material obtained by above coprecipitation method exhibited better electrochemical performance. The method could provide a mass production route at a low cost for its commercial applications.

2. Experimental section

2.1. Material preparation and characterization

During our synthesis of the coprecipitation precursor, 1.314 g $NiSO_4{\cdot}6H_2O$, 2.535 g $MnSO_4{\cdot}H_2O$ were dissolved in 100 ml of distilled water and then stirred continuously for 10 min to form a homogenous solution. After that, 50 ml of anhydrous ethanol were added into the mixed solution mentioned above, stirring continuously for another 5 min until solution A obtained. At the same time, 2.37 g NH_4HCO_3 was dissolved in 50 ml of distilled water to form solution B, it also needed continuous agitation for about 10 min to be completely dissolved. Then solution B was mixed with solution A thoroughly by stirring for only 1 h. In addition, a suitable amount of sodium sulfide solution (about 10–15 drops of 0.03 mol l^{-1} solution) was used as a reagent to reduce the loss of Ni ions dissolved in water because of the complexation with ammonium ions in solution. Finally, the $Ni_{0.25}Mn_{0.75}CO_3$ precipitates were statically settled and aged overnight. The purpose of aging is to make the small crystals disappear and the large grains grow. Then the precipitation was centrifugated and washed with deionized water for four times. At the last time, we used absolute alcohol to replace the water and then put the precipitation in the oven at 80 °C for 12 h.

To verify the effect of the dielectric constant, we changed the proportion of ethanol to water ranging from 1:4, 1:3, 1:2, 1:1, 2:1 to 3:1. The other experiment parameters kept unchanged. The contrastive sample was prepared by a sol-gel method. In this way, 1.244 g Ni $(CH_3COO)_2{\cdot}4H_2O$, 3.676 g $MnSO_4{\cdot}4H_2O$, 4.92 g sucrose and 0.693 g $LiCH_3COO$ were dissolved in 100 ml of deionized water and stirred in the oil bath until the gel appeared.

The cathode material prepared by coprecipitation method was first heated at 500 °C for 2 h and transformed into oxide. After cooling down, the oxide was washed with deionized water, so that a series of impurity ions could be removed, such as sulfur ions. The final product was synthesized by mixed with a stoichiometric amount of Li_2CO_3 (excess 5 wt %) and calcined at 400 °C for 2 h, 600 °C for 2 h and finally 800 °C for 3 h. The control group was annealed at the same calcination condition.

The X-ray diffraction (XRD) patterns were collected via a Rigaku Ultima IV with Cu Ka radiation from 10 to 80° to obtain the information of the structure. Morphology and crystal structure were recorded by scan electron microscopy (SEM, Zeiss SUPRA 55) and high-resolution transmission electron microscopy (HRTEM, JEM–2100). The acceleration voltage of TEM is 200 kV. The Raman measurement was performed by using a Lab Ram HR 800 which was equipped with an Ar^+ laser ($\lambda = 632.8$ nm) micro Raman spectrometer. The elemental information of the sample was tested by X-ray photoelectron spectroscopy (PHI-5000 versaprobe).

2.2. Electrochemical measurements

The electrochemical tests were recorded with CR2032-type coin cells. The active materials were mixed with carbon conductive agent (acetylene black) and polyvinylidene fluoride (PVDF) at the weight ratio of 80: 10: 10. The uniform slurry was tape casted on the coated-carbon aluminum foil and then dried at 80 °C for 12 h. Then the dried foils were cut into circular disks as working electrodes. The loading density was about 1.77 mg cm^{-2}. The electrolyte solution contained 1 M $LiPF_6$ in ethylene carbonate (EC) and dimethyl carbonate (DMC) (1:1 by weight). The Celgard 2400 microporous polypropylene membrane was chosen to be separators. The coin-type cells were fabricated in an argon-filled glovebox with water and oxygen contents under 0.1 ppm. Galvanostatic charge-discharge cycling performance was measured by Land CT 2001 battery tester in the voltage range of 3.5 V–4.95 V (1 C = 146.7 mAh g^{-1}). The electrochemical impedance spectroscopy (EIS) and Cyclic Voltammetry were carried out on an electrochemical workstation (CHI660C) by using a three electrodes cell.

3. Results and discussions

As shown in Scheme 1, during the synthesis of the coprecipitation precursor, we attempted to adopt different proportions of ethanol to water as solvent, and the feature of the precursors had some obvious distinctions. After the high temperature treatment, the final products were quite different. (The micrographs of the precursors and final products are shown in Supplementary Material Fig. S1 and Fig. S2). As is well known, the structure of active materials has an important influence on the performance of cells, so we select an optimal proportion of solvent to synthesize the target LNMO. It is not difficult to find that the ratio of ethanol to water is the most suitable at 1:3. Under this reaction condition, the products could obtain the optimum morphology

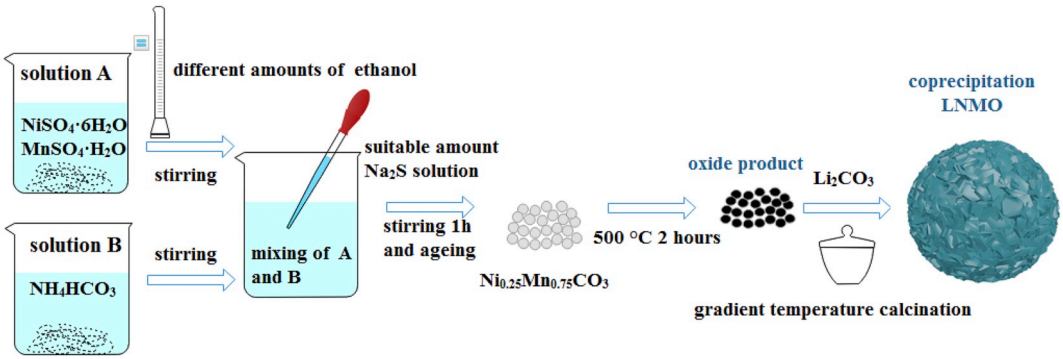

Scheme 1. Schematic diagram of the synthesis route.

retention. This beneficial surface structure makes the active material have large contacts with electrolyte and improve the electrochemical performance.

We can see the micrographs in Fig. 1(a–d), which shows the SEM images of coprecipitation precursors and final products at different magnifications. The diameter of coprecipitation precursors is about 3 μm and maintain pretty well after the gradient heating. The homogeneous spherical morphology does not change. At the same time, a multilevel structure appeared after the high temperature treatment, because the carbonate precursors were decomposed accompanying with large amount of CO_2. The primary particles are in nanoscale, and the secondary particles are in microscale. Such a structure could not only improve the rate performance of the material, but also enhance the cycling performance. The images of (e) and (f) show the sol-gel precursors and the final products after calcination. It is obvious that the control group does not show a homogeneous morphology and scatters unevenly.

The XRD patterns and Rietveld refinements of the coprecipitation products (which is produced by the proportion of ethanol to water for 1:3) and the sol-gel products are shown in Fig. 2(a and b). The two

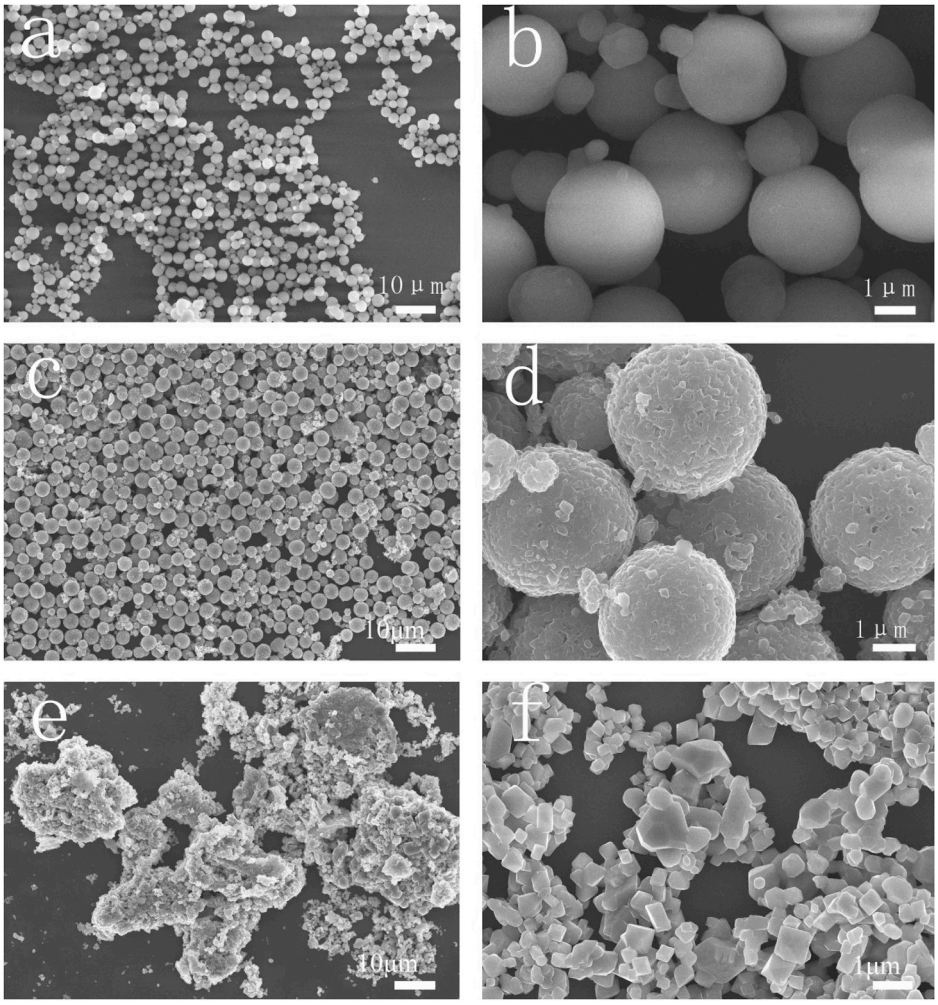

Fig. 1. FESEM images of the samples: (a), (b) $Ni_{0.25}Mn_{0.75}CO_3$ precursors; (c), (d) $LiNi_{0.5}Mn_{1.5}O_4$ products; (e) precursors from sol-gel method; and (f) final products from sol-gel method.

structure of the space group are both $P4_332$-type. We can see clearly that all the peaks can be well indexed as a cubic spinel structure without any impurity phases. The impurities such as $LiNi_xO$ and NiO that may occur during the preparation progress have not appeared in our work [30].

The lattice parameters of the samples were obtained by Rietveld refinement of the XRD data, and the results are shown in Table 1. The reasonably small values of R_{wp} (6.58% for coprecipitation, 8.0% for sol-gel) and R_p (4.89% for coprecipitation, 6.04% for sol-gel) suggest that the fitting results are reliable.

The TEM images were used to further characterize the morphology and the structure of coprecipitation LNMO. As shown in Fig. 3 (a), the material we have made is a solid sphere consisting secondary structure, which is consistent with the SEM result. The HRTEM images presented in (b) shows that the lattice fringe spacing of the coprecipitation products is about 0.48 nm, which evidences the appearance of the facet (111) of the $LiNi_{0.5}Mn_{1.5}O_4$. As we all known, the exposed facets (111) with lower Mn dissolution help to stabilize the surface of the structure, which will exhibit better performance than other planes [31,32].

Fig. 4 displays the Raman spectrum of the coprecipitation LNMO sample. The highest wavenumber band (627 cm^{-1}) is due to the Mn–O stretching vibration. A typical feature for disordered structure of the product can be confirmed by peak which is not obviously splitting at about 597 cm^{-1} [33–35]. It also testifies that we have successfully synthesized a high purity material with the structure of $P4_332$-type LNMO.

Fig. 5 (a) presents the charge and discharge curves of the coprecipitation $LiNi_{0.5}Mn_{1.5}O_4$ cathode at different cycles. The first and second cycles were tested at 0.5 C and the rest were measured at the current density of 1 C (146.7 mAh g^{-1}). The material presented a discharge capacity of about 135 mAh g^{-1} at the first cycle, 140.9 mAh g^{-1} at the tenth cycle, 138.5 mAh g^{-1} at the 50th cycle, 136.8 mAh g^{-1} at 100th cycle and 133.3 mAh g^{-1} at 200th cycle. The dominant discharge voltage plateaus were around 4.7 V, which emerge due to the two pairs of redox couple Ni^{2+}/Ni^{3+}, Ni^{3+}/Ni^{4+}. The test of the Cyclic Voltammetry in Fig. 5 (b) agrees well with the charge-discharge curves. The redox peaks around 4.6–4.9 V correspond to the transformation of Ni^{2+}/Ni^{3+} and Ni^{3+}/Ni^{4+}. Nevertheless, the slight redox peaks appearing at the range of 3.9–4.2 V are associated with the Mn^{3+}/Mn^{4+} redox couple.

Fig. 6 presents the X-ray photoelectron spectroscopy of the coprecipitation of the LNMO sample. Fig. 6 (a) shows the elemental survey results of the sample. The Ni2p is illustrated in Fig. 6 (b), the main peaks located at 854.4 eV and 871.9 eV are corresponding to the binding energy of Ni2p3/2 and Ni2p1/2, which reveal evidence of the existence of Ni^{2+}. And the result of Mn2p shown in Fig. 6 (c) demonstrates the coexistence of Mn^{3+} and Mn^{4+}, where the binding energy of Mn2p3/2 and Mn2p1/2 are located at 641.9 eV, 642.9 eV and 653.9 eV. The results are in agree with the test of CV. Fig. 6 (d) shows the O1s XPS spectra, in which there are two main peaks. The peak at 529.5 eV is a characteristic peak of oxygen atoms in the crystalline network, while the other peak located at 531.4 eV could be assigned to the oxygen absorbed at the surface of the material according to the literature [36].

Fig. 7 (a) shows the cyclic properties of the two materials. The cells were first activated with a small current density of 0.5 C for two loops and then cycled for 200 times at a higher current density of 1 C. The cell assembled by coprecipitation LNMO performed excellent cyclability, retaining 133 mAh g^{-1} after 200 cycles. Furthermore, this active

Table 1
The Rietveld refined structural data obtained from XRD.

Method	a (Å) ($a=b=c$)	V (Å^3)	R_{wp}	R_p
coprecipitation	8.182887	547.92316	6.58%	4.89%
Sol-gel	8.176176	546.57617	8.0%	6.04%

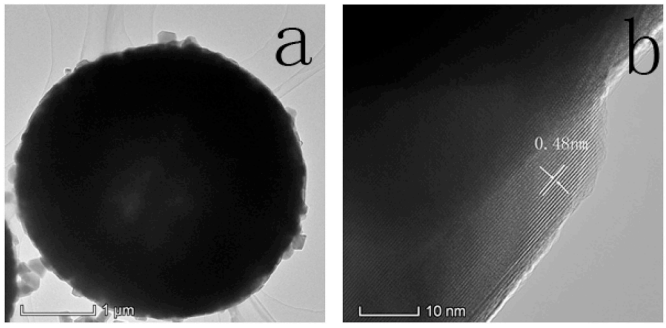

Fig. 3. (a) TEM and (b) HRTEM images of the coprecipitation LNMO product.

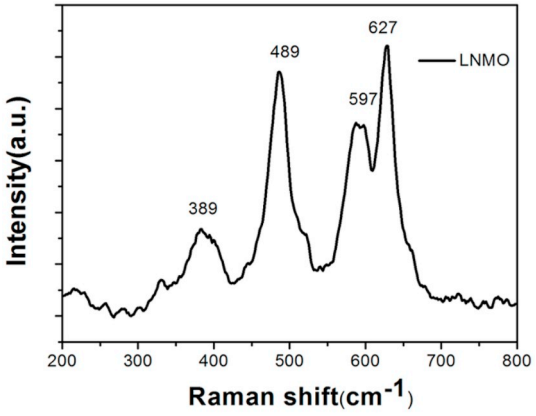

Fig. 4. Raman spectra of the coprecipitation LNMO sample.

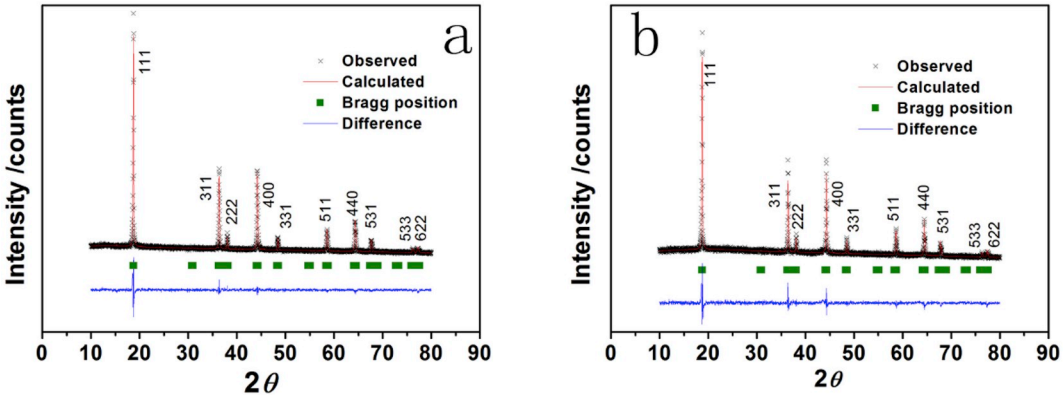

Fig. 2. (a) XRD patterns of the coprecipitation LNMO sample. (b) XRD patterns of the sol-gel LNMO sample.

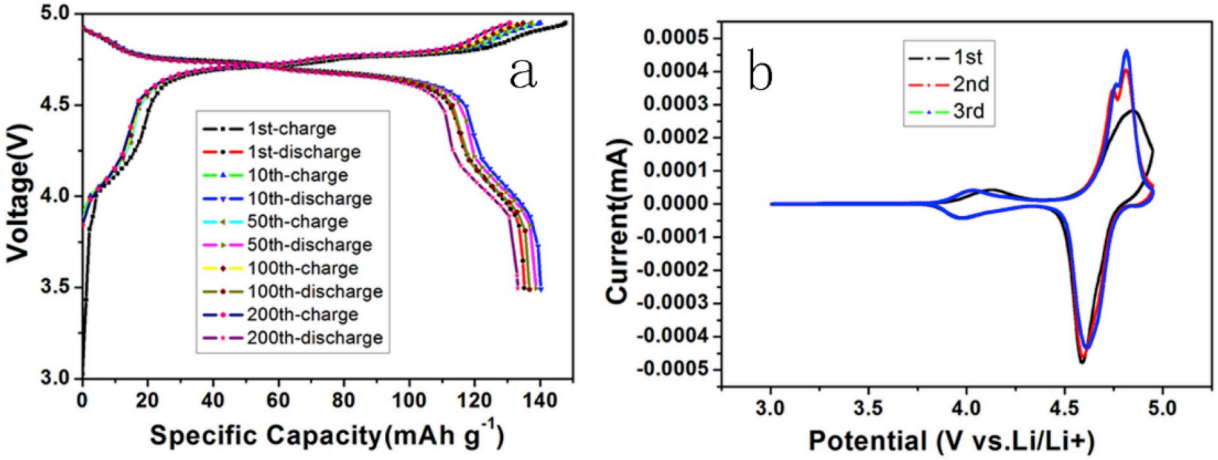

Fig. 5. (a) Different charge and discharge curves of the cells with coprecipitation LNMO cathode materials. (b) Cycling performance of the coprecipitation LNMO product. The charge and discharge current density were 1 C and the voltage range was 3.5–4.95 V.

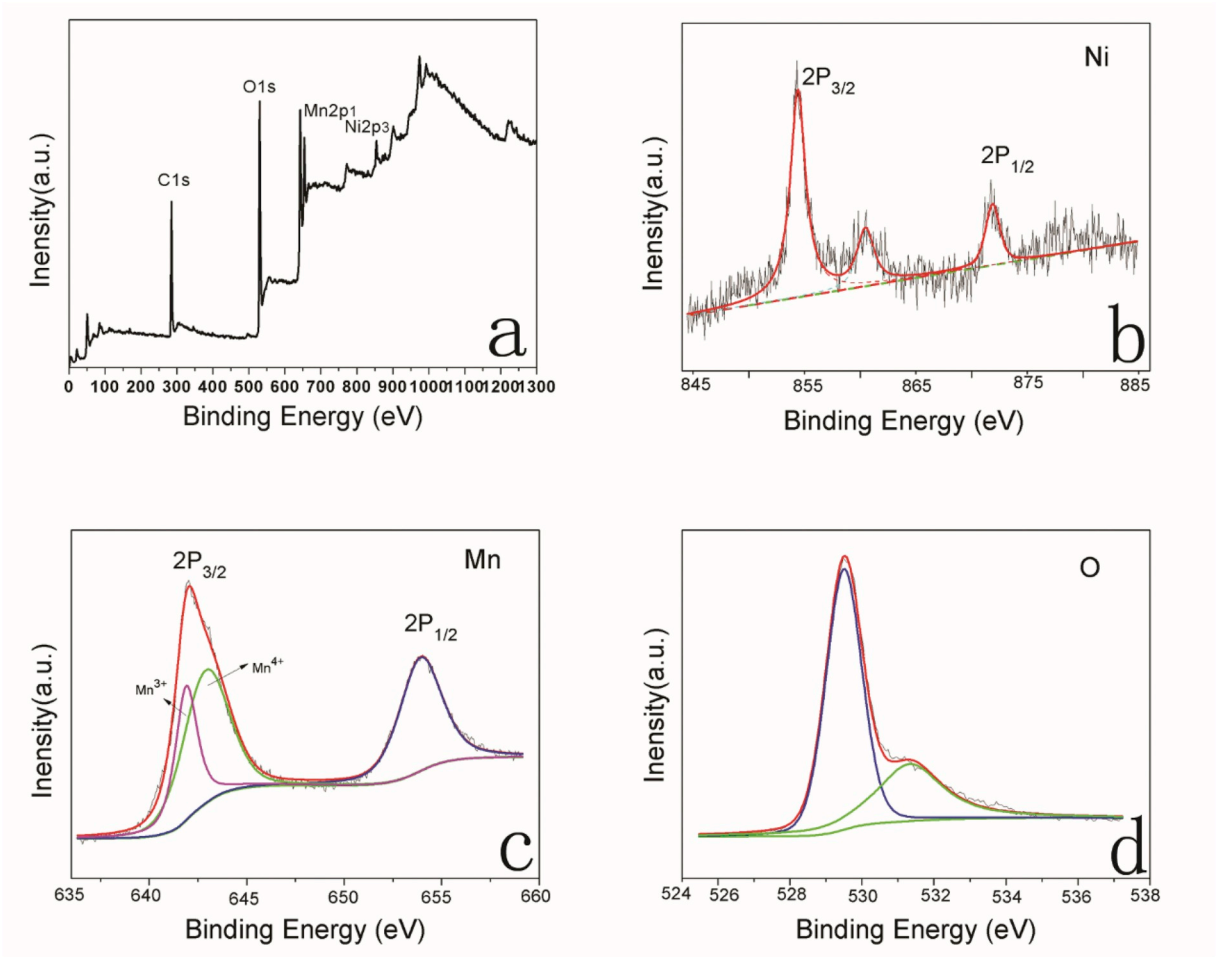

Fig. 6. X-ray photoelectron spectroscopy of the coprecipitation LNMO sample.

material exhibited amazing rate performance with gradual increase of the current density. As is shown in Fig. 7 (b), with the increasing current density from 0.2 C, 0.5 C, 1 C, 2 C, 5 C–10 C, the discharge capacities of the coprecipitation LNMO exhibit 137.3, 135.0, 133.6, 132.5, 127.2, 114 mAh g^{-1} respectively. It is clearly that the materials prepared by coprecipitation method have better rate performance than those prepared by sol-gel method. The excellent electrochemical performance of the coprecipitation LNMO could be attributed to its multistage structure. The nanoscale primary particles could shorten the distance for lithium-ion diffusion, which is crucial to improve the rate performance. And the assembled secondary particles of micro-size assist the structure stability, which contribute to the cycling stability. (The performance comparison with other proportions of ethanol to water is shown in Fig. S3, Supplementary Material). Except for that, we have made some summaries of

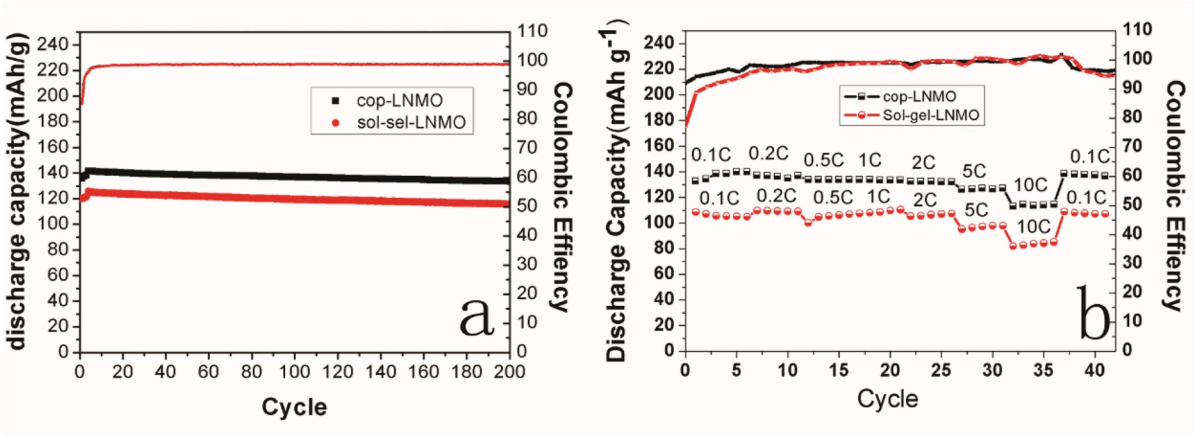

Fig. 7. (a) Cycling tests of both samples at a constant charge-discharge rate at 1 C. (b) Rate properties of the LNMO product.

the cyclic stability in comparison with literatures reported on $LiNi_{0.5}Mn_{1.5}O_4$ samples in Table 2.

To further investigate the application of the coprecipitation LNMO, we fabricated a full cell with $Li_4Ti_5O_{12}$ as anode, as shown in Fig. 8. The N/P (negative to positive) loading ratio for the full cell was about 1.1. The full cell exhibited 125.1 mAh g^{-1} capacity at the first cycle, with an initial coulombic efficiency of 77.7%. Subsequently, it delivered 132.4 mAh g^{-1} capacity at a current density of 1 C and maintained 122.3 mAh g^{-1} after 200 cycles, which offered a capacity retention of 92.4%.

The cathode was also tested at the elevated temperature of 55 °C. As shown in Fig. 9 (a), the normal voltage curve platform is still displayed with the dominant charge discharge voltage plateaus around 4.7 V, which indicates the good stability of our material at elevated temperature. Fig. 9 (b) exhibits stable cycle performance at 55 °C. It presented 132.3 mAh g^{-1} at 1 C and preserved 93.3% after 100 cycles.

Fig. 10 (a) shows the EIS measurements and equivalent circuits of the coprecipitation LNMO and sol-gel LNMO. Generally, the electrolyte resistances (R_s) in the high frequency area were about 1.84 and 2.12 Ω cm^2 before cycle. And the R_s became 19.22 and 33.45 Ω cm^2 after 200 cycles. The fitting results of the charge transfer resistance between electrolyte and electrode (R_{ct}) in middle-high frequency were about 58.92 and 60.17 Ω cm^2 respectively. While after cycle, they became 203.12 and 330.45 Ω cm^2. Obviously, the coprecipitation LNMO sample exhibits the smaller impedance than the sol-gel sample. Fig. 10 (c) shows the impendence at 55 °C. The electrolyte resistances (R_s) were 6.48 and 12.54 Ω cm^2 before and after cycling. The charge transfer resistance between electrolyte and electrode (R_{ct}) in middle-high frequency were about 99.45 and 280.38 Ω cm^2 before and after cycling. The impendences became larger, which may be attributed to severe electrolyte/cathode interface reaction at elevated temperatures [37].

Table 2
Summary of the cyclic stability about $LiNi_{0.5}Mn_{1.5}O_4$ samples already published and our work. (1 C = 146.7 mA h g^{-1}).

Preparation method	Rate/Cycle number	Discharge Capacity and Retention after cycle	Reference
Hydrothermal	1 C/30	135 mAh g^{-1} 98%	10
Hydrothermal	0.5C/100	115 mAh g^{-1} 85%	11
Sol-gel method	1 C/200	121 mAh g^{-1} 91.7%	12
Sol-gel method	1C/100	130 mAh g^{-1} 94%	13
template method	1 C/100	125 mAh g^{-1} 96.6%	14
template method	1 C/200	100 mAh g^{-1} 70%	15
spray drying	0.15 C/50	135 mAh g^{-1} 97%	16
spray drying	2C/50	119 mAh g^{-1} 98%	17
solid-state	0.5 C/100	129 mAh g^{-1} 96.3%	23
solid-state	1 C/100	135 mAh g^{-1} 96.4%	24
coprecipitation	0.5C/100	135 mAh g^{-1} 95%	18
coprecipitation	1 C/200	129 mAh g^{-1} 94%	19
coprecipitation	1 C/200	133 mAh g^{-1} 94.2%	This work

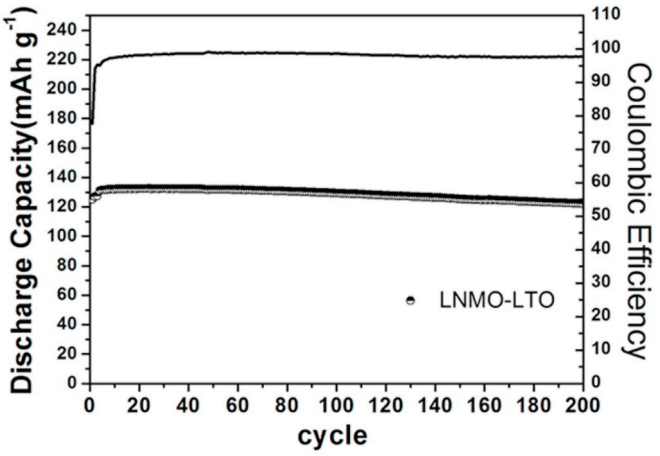

Fig. 8. The cycling performance of the coprecipitation LNMO/LTO full cells at 1 C.

The straight line in the low frequency region presents Warburg diffusion which is related to the diffusion of Li^+ in the electrode materials. So we also calculated the Li^+ diffusion coefficient (D_{Li}) according to the formula of $D_{Li} = R^2T^2/2A^2n^2F^4C^2\sigma^2$. In the formula, D_{Li} stands for the Li^+ diffusion coefficient in the material (cm^2/s), T is the absolute temperature (298.15 K), R means the gas constant (8.31 J/mol·K), A is the surface area of the cathode electrode (it is about 1.13 cm^2), n is the number of electrons transferred per molecule during the electrochemical reaction, F is the Faraday constant (96485 C/mol), and C is the molar concentration of Li^+ in the product which comes from the refined XRD data of the cell volume in Table 1 (about 1.212×10^{-2} mol/cm^3 for the coprecipitation and 1.215×10^{-2} mol/cm^3 for the sol-gel), and σ is the Warburg factor associated with Z_{Re} ($Z_{Re} \propto \omega^{-1/2}$) [38]. Fig. 10 (b) shows the relationship between Z_{Re} and the reciprocal square root of frequency ($\omega^{-1/2}$) in the low frequency region at 25 °C. The σ values of the LNMO samples were calculated to be 1.90, 2.98, 14.55 and 23.11 Ω $s^{-1/2}$ respectively. Therefore, the D_{Li} values of the products were 5.24×10^{-11} cm^2/s, 2.11×10^{-11} cm^2/s, 2.67×10^{-12} cm^2/s and 4.7×10^{-13} cm^2/s, which means that the material produced by our coprecipitation method exhibits a better capability to diffuse and transmit lithium ions. It can be attributed to the multilevel structure. Fig. 10 (d) shows the relationship at 55 °C. The calculated D_{Li} of the products were 9.6×10^{-13} cm^2/s and 3.5×10^{-13} cm^2/s. R_s, R_{ct}, and D_{Li} are shown in Table 3.

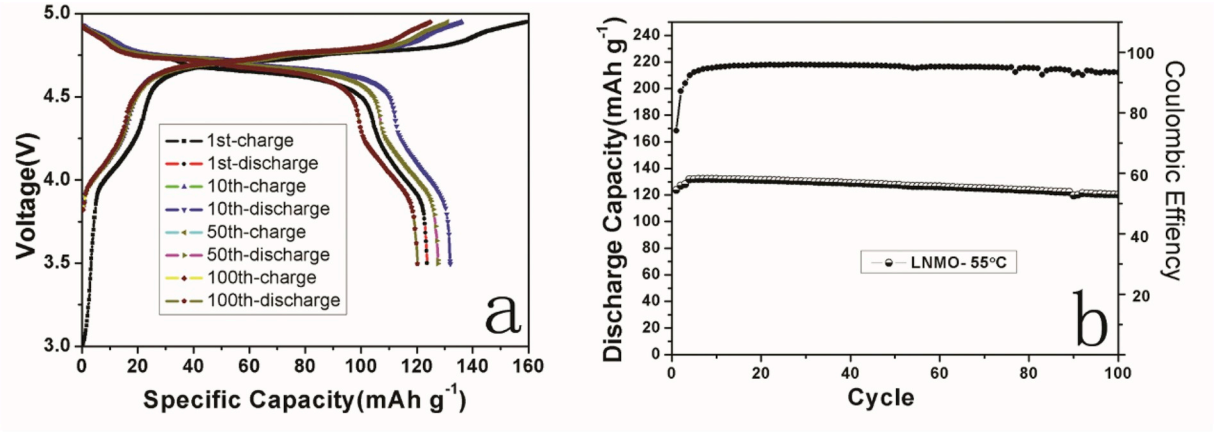

Fig. 9. (a) Charge and discharge curves of the cells with coprecipitation LNMO cathode at 55 °C. (b) Cycling performance of the coprecipitation LNMO product. The charge and discharge current density were 1 C at 55 °C.

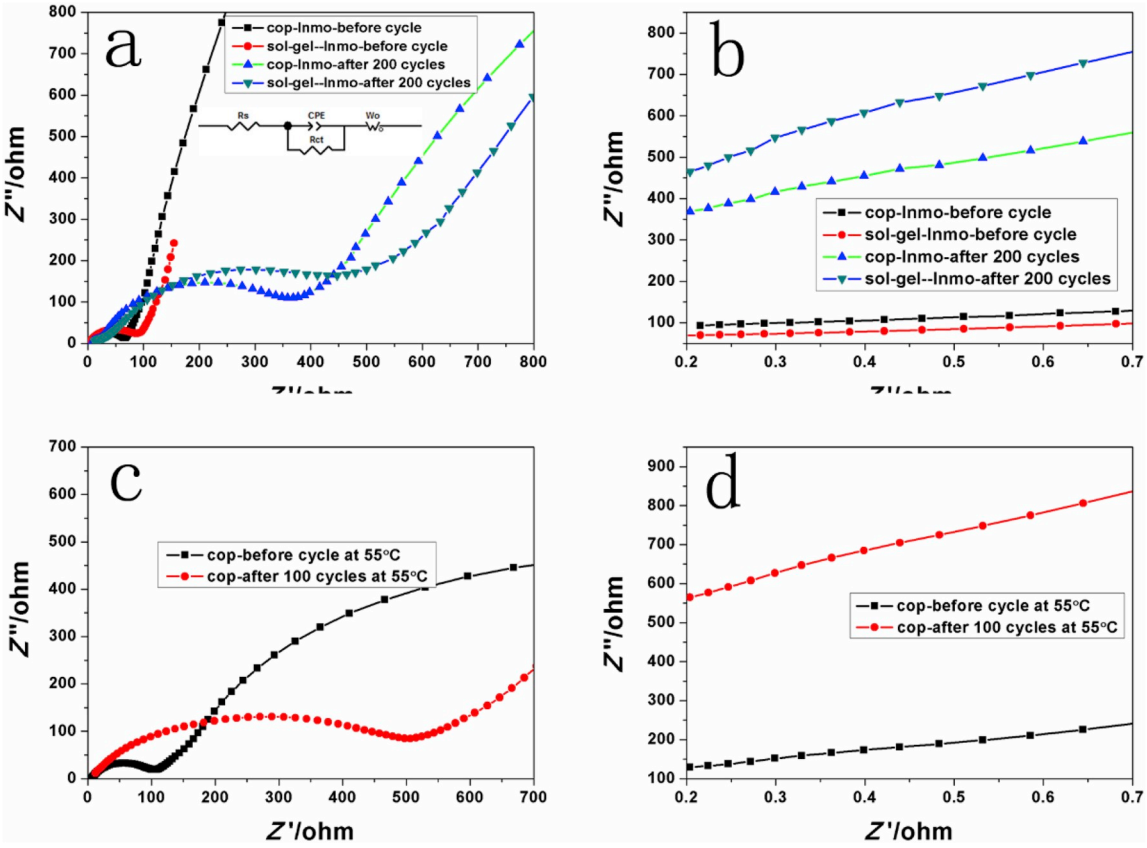

Fig. 10. (a) EIS spectra of the samples before and after 200 cycles in the frequency range from 100 kHz to 0.01 Hz at 25 °C and the equivalent circuit. (b) Relationship between Z_{Re} and square root of frequency ($\omega^{-1/2}$) in a low frequency region. (c) EIS spectra of the samples at 55 °C before and after 100 cycles in the frequency range from 100 kHz to 0.01 Hz. (d) Relationship between Z_{Re} and square root of frequency ($\omega^{-1/2}$) in a low frequency region.

4. Conclusion

By using water and ethanol as cosolvent for coprecipitation, we prepared spherical multilevel structure LNMO after a simple calcination. The variation of cosolvent has nonnegligible effect on the structure and electrochemical performance of final products. When the proportion of ethanol to water was adjusted to a suitable value, the dielectric constant of solution obtained a moderate reduction, accompanying with the elevation of precipitation rate. On this basis, we can rapidly prepare the precursors in an hour. When used as a cathode for lithium ion batteries, the LNMO product exhibited a capacity of 141 mAh g^{-1} at 1 C and 114 mAh g^{-1} even at 10 C. It showed a retention of 94.2% after 200 cycles. A full cell with $Li_4Ti_5O_{12}$ was assembled and delivered superior matching performance. It reached a capacity over 132 mAh g^{-1} at 1 C and a high retention of 92.4% after 200 cycles. The high electrochemical performance could be attributed to its multistage structure. Even at the elevated temperature of 55 °C, the material presented good performance with 133.2 mAh g^{-1} and maintained 93.3% after 100 cycles. Considering about the convenience of synthesis and the outstanding electrochemical performance of LNMO, we believe that it is promising for commercial applications.

Table 3
The impendence and the D_{Li} of the products.

Methods	Condition	D_{Li} cm^2/s	R_s Ω cm	R_{ct} Ω cm
Coprecipitation	Before cycle at 25 °C	5.24×10^{-11}	1.84	58.92
Sol-gel	Before cycle at 25 °C	2.11×10^{-11}	2.12	60.17
Coprecipitation	After 200 cycles at 25 °C	2.67×10^{-12}	19.22	203.12
Sol-gel	After 200 cycles at 25 °C	4.7×10^{-13}	33.45	330.45
Coprecipitation	Before cycle at 55 °C	9.6×10^{-13}	6.48	99.45
Coprecipitation	After 100 cycles at 55 °C	3.5×10^{-13}	12.54	280.38

Acknowledgements

This work was supported by the National Natural Science Foundation of China [No. 61574118]; and the Key Project of Science and Technology Plan of Fujian Province [Grant No. 2015H0038].

Appendix A. Supplementary data

Supplementary data to this article can be found online at https://doi.org/10.1016/j.matchemphys.2019.122137.

References

[1] M. Armand, J.M. Tarascon, Building better batteries, Nature 451 (2008) 652–657.
[2] B. Dunn, H. Kamath, J.M. Tarascon, Electrical energy storage for the grid: a battery of choices, Science 334 (2011) 928–935.
[3] X. Zhang, F. Cheng, J. Yang, J. Chen, $LiNi_{0.5}Mn_{1.5}O_4$ porous nanorods as high-rate and long-life cathodes for Li-ion batteries, Nano Lett. 13 (2013) 2822–2825.
[4] J. Li, M. Li, L. Zhang, J. Wang, General synthesis of xLi2MnO3·(1 − x)$LiNi_{1/3}Co_{1/3}Mn_{1/3}O_2$ (x = 1/4, 1/3, and 1/2) hollow microspheres towards enhancing the performance of rechargeable lithium ion batteries, J. Mater. Chem. A 4 (2016) 12442–12450.
[5] Z. Xing, X. Luo, Y. Qi, W.F. Stickle, K. Amine, J. Lu, X. Ji, Nitrogen-Doped nanoporous graphenic carbon: an efficient conducting support for O_2 cathode, ChemNanoMat 2 (2016) 692–697.
[6] Z. Xing, G. Li, S. Sy, Z. Chen, Recessed deposition of TiN into N-doped carbon as a cathode host for superior Li-S batteries performance, Nano Energy 54 (2018) 1–9.
[7] Z. Xing, J. Lu, X. Ji, A brief review of metallothermic reduction reactions for materials preparation, Small Methods 2 (2018).
[8] G.B. Zhong, Y.Y. Wang, Z.C. Zhang, C.H. Chen, Effects of Al substitution for Ni and Mn on the electrochemical properties of $LiNi_{0.5}Mn_{1.5}O_4$, Electrochim. Acta 56 (2011) 6554–6561.
[9] J. Xiao, X. Chen, P.V. Sushko, M.L. Sushko, L. Kovarik, J. Feng, Z. Deng, J. Zheng, G.L. Graff, Z. Nie, D. Choi, J. Liu, J.G. Zhang, M.S. Whittingham, High-performance $LiNi_{0.5}Mn_{1.5}O_4$ spinel controlled by Mn^{3+} concentration and site disorder, Adv. Mater. 24 (2012) 2109–2116.
[10] Y. Liu, M. Zhang, Y. Xia, B. Qiu, Z. Liu, X. Li, One-step hydrothermal method synthesis of core–shell $LiNi_{0.5}Mn_{1.5}O_4$ spinel cathodes for Li-ion batteries, J. Power Sources 256 (2014) 66–71.
[11] E. Zhao, L. Wei, Y. Guo, Y. Xu, W. Yan, D. Sun, Y. Jin, Rapid hydrothermal and post-calcination synthesis of well-shaped $LiNi_{0.5}Mn_{1.5}O_4$ cathode materials for lithium ion batteries, J. Alloy. Comp. 695 (2017) 3393–3401.
[12] O. Sha, S. Wang, Z. Qiao, W. Yuan, Z. Tang, Q. Xu, Y. Su, Synthesis of spinel $LiNi_{0.5}Mn_{1.5}O_4$ cathode material with excellent cycle stability using urea-based sol–gel method, Mater. Lett. 89 (2012) 251–253.
[13] M.C. Kim, K.W. Nam, E. Hu, X.Q. Yang, H. Kim, K. Kang, V. Aravindan, W.S. Kim, Y.S. Lee, Sol-gel synthesis of aliovalent vanadium-doped $LiNi_{0.5}Mn_{1.5}O_4$ cathodes with excellent performance at high temperatures, ChemSusChem 7 (2014) 829–834.
[14] G. Liu, X. Kong, H. Sun, B. Wang, Z. Yi, Q. Wang, A facile template method to synthesize significantly improved $LiNi_{0.5}Mn_{1.5}O_4$ using corn stalk as a bio-template, Electrochim. Acta 141 (2014) 141–148.
[15] X. Liu, D. Li, Q. Mo, X. Guo, X. Yang, G. Chen, S. Zhong, Facile synthesis of aluminum-doped $LiNi_{0.5}Mn_{1.5}O_4$ hollow microspheres and their electrochemical performance for high-voltage Li-ion batteries, J. Alloy. Comp. 609 (2014) 54–59.
[16] D. Li, A. Ito, K. Kobayakawa, H. Noguchi, Y. Sato, Electrochemical characteristics of $LiNi_{0.5}Mn_{1.5}O_4$ prepared by spray drying and post-annealing, Electrochim. Acta 52 (2007) 1919–1924.
[17] T. Risthaus, J. Wang, A. Friesen, A. Wilken, D. Berghus, M. Winter, J. Li, Synthesis of spinel $LiNi_{0.5}Mn_{1.5}O_4$ with secondary plate morphology as cathode material for lithium ion batteries, J. Power Sources 293 (2015) 137–142.
[18] D. Lu, L. Yuan, Z. Chen, R. Zeng, Y. Cai, Co-precipitation preparation of $LiNi_{0.5}Mn_{1.5}O_4$ hollow hierarchical microspheres with superior electrochemical performance for 5 V Li-ion batteries, J. Alloy. Comp. 730 (2018) 509–515.
[19] Z. Zhu, Qilu, D. Zhang, H. Yu, Preparation of spherical hierarchical $LiNi_{0.5}Mn_{1.5}O_4$ with high electrochemical performances by a novel composite co-precipitation method for 5V lithium ion secondary batteries, Electrochim. Acta 115 (2014) 290–296.
[20] X. Zhu, X. Li, Y. Zhu, S. Jin, Y. Wang, Y. Qian, Porous $LiNi_{0.5}Mn_{1.5}O_4$ microspheres with different pore conditions: preparation and application as cathode materials for lithium-ion batteries, J. Power Sources 261 (2014) 93–100.
[21] M. Zhang, J. Wang, Y. Xia, Z. Liu, Microwave synthesis of spherical spinel $LiNi_{0.5}Mn_{1.5}O_4$ as cathode material for lithium-ion batteries, J. Alloy. Comp. 518 (2012) 68–73.
[22] L. Wang, G. Liu, W. Wu, D. Chen, G. Liang, Synthesis of porous peanut-like $LiNi_{0.5}Mn_{1.5}O_4$ cathode materials through an ethylene glycol-assisted hydrothermal method using urea as a precipitant, J. Mater. Chem. A 3 (2015) 19497–19506.
[23] N.M. Hagh, G.G. Amatucci, A new solid-state process for synthesis of $LiMn_{1.5}Ni_{0.5}O_{4-\delta}$ spinel, J. Power Sources 195 (2010) 5005–5012.
[24] X.Y. Feng, C. Shen, X. Fang, C.H. Chen, Synthesis of $LiNi_{0.5}Mn_{1.5}O_4$ by solid-state reaction with improved electrochemical performance, J. Alloy. Comp. 509 (2011) 3623–3626.
[25] J.H. Kim, A. Huq, M. Chi, N.P.W. Pieczonka, E. Lee, C.A. Bridges, M.M. Tessema, A. Manthiram, K.A. Persson, B.R. Powell, Integrated nano-domains of disordered and ordered spinel phases in $LiNi_{0.5}Mn_{1.5}O_4$ for Li-ion batteries, Chem. Mater. 26 (2014) 4377–4386.
[26] Y.-K. Sun, S.W. Oh, C.S. Yoon, H.J. Bang, J. Prakash, Effect of sulfur and nickel doping on morphology and electrochemical performance of $LiNi_{0.5}Mn_{1.5}O_4$−xSx spinel material in 3-V region, J. Power Sources 161 (2006) 19–26.
[27] G. Ma, S. Li, W. Zhang, Z. Yang, S. Liu, X. Fan, F. Chen, Y. Tian, W. Zhang, S. Yang, A general and mild approach to controllable preparation of manganese-based micro- and nanostructured bars for high performance lithium-ion batteries, Angew. Chem. Int. Ed. 55 (2016) 3667–3671.
[28] G. Akerlof, Dielectric constants of some organic solvent-water mixtures at various temperatures, J. Am. Chem. Soc. 54 (1932) 4125–4139.
[29] H.-I. Chen, H.-Y. Chang, Homogeneous precipitation of cerium dioxide nanoparticles in alcohol/water mixed solvents, Colloids Surf., A 242 (2004) 61–69.
[30] L. Wang, H. Li, X. Huang, E. Baudrin, A comparative study of Fd-3m and P4332 "$LiNi_{0.5}Mn_{1.5}O_4$", Solid State Ion. 193 (2011) 32–38.
[31] Y. Wu, C. Cao, J. Zhang, L. Wang, X. Ma, X. Xu, Hierarchical $LiMn_2O_4$ hollow cubes with exposed {111} planes as high-power cathodes for lithium-ion batteries, ACS Appl. Mater. Interfaces 8 (2016) 19567–19572.
[32] W. Sun, F. Cao, Y. Liu, X. Zhao, X. Liu, J. Yuan, Nanoporous $LiMn_2O_4$ nanosheets with exposed {111} facets as cathodes for highly reversible lithium-ion batteries, J. Mater. Chem. 22 (2012).
[33] N. Amdouni, K. Zaghib, F. Gendron, A. Mauger, C.M. Julien, Structure and insertion properties of disordered and ordered $LiNi_{0.5}Mn_{1.5}O_4$ spinels prepared by wet chemistry, Ionics 12 (2006) 117–126.
[34] X. Zhang, F. Cheng, K. Zhang, Y. Liang, S. Yang, J. Liang, J. Chen, Facile polymer-assisted synthesis of $LiNi_{0.5}Mn_{1.5}O_4$ with a hierarchical micro-nano structure and high rate capability, RSC Adv. 2 (2012) 5669–5675.
[35] Y. Pei, C.-Y. Xu, Y.-C. Xiao, Q. Chen, B. Huang, B. Li, S. Li, L. Zhen, G. Cao, Phase transition induced synthesis of layered/spinel heterostructure with enhanced electrochemical properties, Adv. Funct. Mater. 27 (2017).
[36] L. Li, J. Sui, J. Chen, Y. Lu, $LiNi_{0.5}Mn_{1.5}O_4$ microrod with ultrahigh Mn^{3+} content: a high performance cathode material for lithium ion battery, Electrochim. Acta 305 (2019) 433–442.
[37] X. Cao, X. He, J. Wang, H. Liu, S. Roser, B.R. Rad, M. Evertz, B. Streipert, J. Li, R. Wagner, M. Winter, I. Cekic-Laskovic, High voltage $LiNi_{0.5}Mn_{1.5}O_4$/$Li_4Ti_5O_{12}$ lithium ion cells at elevated temperatures: carbonate- versus ionic liquid-based electrolytes, ACS Appl. Mater. Interfaces 8 (2016) 25971–25978.
[38] X. Ju, H. Huang, W. He, H. Zheng, P. Deng, S. Li, B. Qu, T. Wang, Surfactant-Assisted synthesis of high energy {010} facets beneficial to Li-ion transport kinetics with layered $LiNi_{0.6}Co_{0.2}Mn_{0.2}O_2$, ACS Sustain. Chem. Eng. 6 (2018) 6312–6320.